[23]G. W. Tichelaar and D. Lazarus, Phys. Rev. 113, 438 (1959).
[24]R. E. Hanneman, R. E. Ogilvie, and H. C. Gatos, Trans. Met. Soc. AIME 233, 691 (1965).
[25]E. D. Albrecht and C. T. Tomizuka, J. Appl. Phys. 35, 3560 (1964).
[26]S. G. Fishman and R. N. Jeffery, Phys. Rev. B 3, 4424 (1971).
[27]D. N. Yoon and D. Lazarus, Bull. Am. Phys. Soc. 15, 381 (1970); D. Lazarus, D. N. Yoon, and R. N. Jeffery, Z. Naturforsch. 26a, 55 (1971); *Atomic Transport in Solids and Liquids* (Stechert-Hafner, New York (1971), p. 311; D. N. Yoon and D. Lazarus, Phys. Rev. B 5, 4934 (1972).
[28]N. F. Mott, Proc. Phys. Soc. (London) 49, 258 (1937).
[29]H. Asano, Y. Bando, N. Nakanishi, and S. Kachi, Trans. Japan Inst. Metals 8, 180 (1967).
[30]H. Iwasaki and T. Uesugi, J. Phys. Soc. Japan 25, 1640 (1968).
[31]*Table of Periodic Properties of the Elements* (E. H. Sargent Co., Chicago, Ill., 1962).

PHYSICAL REVIEW B VOLUME 6, NUMBER 12 15 DECEMBER 1972

Lattice Dynamics of YZn

T. S. Prevender,* S. K. Sinha, and J. F. Smith
Ames Laboratory-U. S. Atomic Energy Commission and Department of Metallurgy, Iowa State University, Ames, Iowa 50010
(Received 30 June 1972)

Phonon dispersion curves for YZn along the (0, 0, ζ), (ζ, ζ, 0), (ζ, ζ, ζ), and ($\frac{1}{2}$, $\frac{1}{2}$, ζ) directions have been measured by inelastic neutron scattering at room temperature. A sixth-neighbor force-constant model was used to obtain a fit to the data; there is residual indication of weak forces of still longer range. The frequency distribution function, Debye temperature as a function of temperature, and mean-square atomic displacements were calculated from the model. No Kohn-type anomaly was observed, and YZn was not found to become superconducting down to 1.2 K. Comparison of the dispersion curves of YZn with those of β-brass shows some pronounced differences, though there is a coincidence of accidental degeneracy between the transverse acoustical and transverse optical branches in both materials at (0, 0, $\frac{1}{2}$).

I. INTRODUCTION

The elucidation of phonon dispersion curves and vibrational spectra from inelastic-neutron-scattering (INS) measurements has been done for a number of materials, but relatively little work has been done on metallic materials involving both lattices with bases and two different atomic species. The first such study was of β-brass (formula CuZn with the cubic CsCl-type structure) by Gilat and Dolling.[1] In the case of β-brass, the over-all shapes of the dispersion curves were found to be quite similar to those which would be expected for a simple bcc element. Because of the small mass difference between copper and zinc atoms, only two of the theoretically expected splittings between the acoustical and optical branches of the dispersion curves at the Brillouin-zone boundaries were large enough to be observed. The present investigation was undertaken to look further at another CsCl-type structure. Initial attention was given to the phase[2] AuZn which is congruently melting at 725 °C. The valence-electron configuration in gold should be closely analogous to that in copper and the primary difference between AuZn and CuZn was expected to be the mass difference between gold and copper. A suitable single crystal of AuZn was grown, and an ultrasonic technique was used for the determination of the elastic constants.[3] Some initial neutron scattering data were accumulated, but it soon became apparent that the absorptivity of AuZn for neutrons was more severe than anticipated. As a result, the requisite time at the neutron flux levels of the presently available reactor was considered too costly to justify the accumulation of sufficient data for a complete delineation of the dispersion curves.

An alternative material had, therefore, to be selected, and the phase YZn was chosen. This phase also crystallizes[4] with the CsCl-type structure. Selection of YZn as the test material sacrificed the advantageous similarity in valence-electron configuration that exists between AuZn and CuZn, but retention of zinc as the second component did at least maintain a common factor. The dominant consideration in the selection of YZn was the favorable ratio that was indicated between neutron scattering and neutron absorption. Thermal neutron cross sections have been tabulated[5] for yttrium as 1.28 ± 0.02 b for absorption, 7.60 ± 0.06 b for coherent scattering, and 0.05 ± 0.03 b for incoherent scattering, and for zinc as 1.1 ± 0.04 b for absorption and 4.1 ± 0.1 b for coherent scattering. The neutron cross sections are colligative, so the favorable scattering-to-absorption ratios for the elements are also characteristic of

the compound YZn. During the experimental acquisition of the inelastic-neutron-scattering data, this favorable ratio resulted in relatively intense phonon peaks.

II. PROCEDURE AND RESULTS

Zinc of 99.999*% purity was purchased from Cominco American Inc., and yttrium near 99.9% purity was generously supplied by J. Croat and Dr. F. H. Spedding of the Ames laboratory. An equiatomic alloy was prepared by placing 53.6255 ± 0.0001 g of yttrium and 39.4335 ± 0.0001 g of zinc in a pointed, 1-in.-diam tantalum crucible. A lid was sealed onto this crucible with an electron-beam welder under reduced pressure of ~ 5 $\times 10^{-5}$ Torr. The tantalum crucible was in turn encapsulated in stainless steel. Chiotti *et al.*[6] have reported that YZn melts congruently at 1105 °C. The alloy was therefore homogenized by agitation in a rocking furnace for 2 h at 1135 °C. The tantalum crucible was subsequently removed from the stainless-steel capsule and placed in a Bridgman furnace. In this Bridgman furnace the tantalum was protected from atmospheric reaction by maintaining reduced pressure of ~ 10^{-6} Torr. The YZn was remelted and then lowered through a temperature gradient of 200 °C/in. at a rate of 0.08 in./h. After removal of the YZn specimen from the tantalum crucible, the specimen was etched with an H_2O_2-HNO_3 mixture; no grain boundaries were detected. Single crystallinity was confirmed by x-ray diffraction, and crystal orientation was determined by the back-reflection Laue technique. The volume of the crystal was about 16 cm^3. The degree of atomic order in the crystal was also checked by x-ray diffraction with an *XRD*-6 single-crystal orienter. Because it was necessary to cut a (100) face on the crystal, this check was made after completion of the neutron scattering measurements. Integrated intensities of (h00) Bragg reflections through 12th order were determined by the step-scan technique. Analysis of these intensity data showed no experimentally detectable atomic disorder. A high degree of atomic order has subsequently been corroborated by Jan,[7] who has observed de Haas–van Alphen oscillations in a specimen from this crystal.

Inelastic-neutron-scattering measurements were made on the YZn crystal with the triple-axis spectrometer at the Ames Laboratory Research Reactor. These measurements were made in the constant-Q mode of operation[8] with fixed incident neutron energy. All measurements were made at room temperature with monochromated wavelengths of either 1.265 or 1.617 Å. The large majority of the phonons were observed with the shorter wavelength, but a few of the low-frequency phonons were observed with the longer wavelength. Data were accumulated for a total of 108 phonons along the 18 branches of the dispersion curves for the (ζ, 0, 0), (ζ, ζ, 0), (ζ, ζ, ζ), and ($\frac{1}{2}$, $\frac{1}{2}$, ζ) directions. Because of generally better instrumental resolution, most of the 108-phonon scans were done with neutron energy loss, i.e., phonon-creation processes. In a very few instances, better access to some of the optical phonons was afforded by scans with neutron energy gain, i.e., phonon-annihilation processes.

A representative phonon profile is shown in Fig. 1. Phonon frequencies were evaluated by utilizing a computer to fit each individual phonon peak, together with background,[9] to a sum of Gaussian functions of adjustable magnitude, position, width, and base ordinate. This at least partially compensates for extraneous contributions to the peak, e.g., elastic and inelastic incoherent contamination. Possible errors arising from asymmetry were reduced by choosing the centroid of the neutron distribution as determining the peak position. Uncertainties in the phonon frequencies were estimated from the statistical errors in the positions that were obtained in this manner. In those cases where several equivalent measurements of the same phonon were carried out under different conditions, the composite data were combined to evaluate the phonon frequency and uncertainty. Table I lists values and uncertainties for 111 phonons; 108 of these result from the inelastic-neutron-scattering measurements and the remaining three are derived for low-frequency acoustical phonons from measurements of ultrasonic wave velocities in the [110] direction.

III. EXPERIMENTAL DATA ANALYSIS

The experimental values for the phonon frequencies represent points on the various branches of

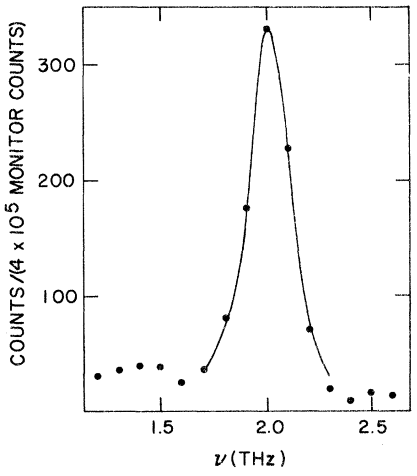

FIG. 1. Typical phonon profile, in this case the TA_1 phonon along the (ζ, ζ, 0) direction with $\zeta = 0.198$.

TABLE I. Phonon frequencies and estimated errors of normal modes at 295 K (units of THz).

ζ	ν	$\delta\nu$	ζ	ν	$\delta\nu$
	LA (0, 0, ζ)			TA_2 (ζ, ζ, 0)	
0.150	1.61	0.03	0.005[a]	0.04	0.01
0.200	2.08	0.04	0.200	1.34	0.04
0.250	2.43	0.04	0.250	1.61	0.04
0.300	2.64	0.04	0.300	1.80	0.04
0.350	2.93	0.06	0.350	1.85	0.04
0.400	3.04	0.05	0.400	1.86	0.03
0.450	3.15	0.06	0.450	1.75	0.08
0.500	3.20	0.04			
				TO_2 (ζ, ζ, 0)	
	LO (0, 0, ζ)		0.0	4.48	0.07
0.150	4.48	0.05	0.102	4.51	0.05
0.250	4.38	0.03	0.202	4.60	0.10
0.300	4.29	0.03	0.302	4.80	0.10
0.400	4.30	0.06	0.402	4.87	0.05
0.500	4.28	0.10			
				LA (ζ, ζ, ζ)	
	TA (0, 0, ζ)		0.098	2.08	0.03
0.250	1.92	0.04	0.123	2.55	0.03
0.300	2.30	0.02	0.148	2.95	0.03
0.350	2.61	0.04	0.250	2.79	0.08
0.400	2.92	0.03	0.300	2.58	0.05
0.450	3.19	0.03	0.350	2.65	0.05
0.500	3.48	0.05	0.400	2.89	0.05
			0.450	3.17	0.05
	TO (0, 0, ζ)		0.500	3.31	0.07
0.050	4.54	0.06			
0.150	4.46	0.03		LO (ζ, ζ, ζ)	
0.250	4.33	0.05	0.000	4.48	0.05
0.350	4.07	0.05	0.050	4.48	0.05
0.450	3.73	0.05	0.100	4.24	0.05
0.500	3.48	0.05	0.150	3.98	0.03
			0.250	3.97	0.06
			0.300	4.37	0.07
			0.350	4.69	0.08
			0.400	4.76	0.06
	LA (ζ, ζ, 0)		0.450	4.74	0.05
0.010[a]	0.18	0.01		TA (ζ, ζ, ζ)	
0.200	3.24	0.05	0.100	1.09	0.03
0.304	3.12	0.03	0.150	1.64	0.03
0.354	2.68	0.03	0.200	2.12	0.04
0.400	2.16	0.04	0.250	2.63	0.04
0.450	1.96	0.03	0.300	3.04	0.07
0.500	1.86	0.05	0.350	3.20	0.05
			0.400	3.25	0.05
	LO (ζ, ζ, 0)		0.450	3.33	0.06
0.080	4.44	0.03	0.500	3.37	0.07
0.160	4.20	0.03			
0.250	3.99	0.08		TO (ζ, ζ, ζ)	
0.300	4.25	0.04	0.000	4.69	0.03
0.350	4.58	0.04	0.100	4.63	0.03
0.425	4.98	0.04	0.200	4.62	0.05
0.500	5.27	0.05	0.300	4.74	0.04
			0.400	4.86	0.05
			0.500	4.90	0.05
				ΠA ($\frac{1}{2}$, $\frac{1}{2}$, ζ)	
	TA_1 (ζ, ζ, 0)		0.100	1.90	0.08
0.010[a]	0.11	0.01	0.200	2.25	0.05
0.148	1.58	0.03	0.300	2.75	0.05
0.198	1.99	0.03	0.400	3.20	0.04
0.248	2.28	0.03			
0.298	2.29	0.03		Π0 ($\frac{1}{2}$, $\frac{1}{2}$, ζ)	
0.347	2.29	0.03	0.200	5.04	0.08
0.398	2.17	0.03	0.300	5.00	0.05
0.447	1.96	0.03	0.400	4.85	0.05
0.500	1.82	0.03			
				ΛA ($\frac{1}{2}$, $\frac{1}{2}$, ζ)	
	TO_1 (ζ, ζ, 0)		0.100	2.40	0.07
0.050	4.47	0.03	0.300	3.65	0.10
0.150	4.27	0.03	0.400	3.40	0.10
0.250	3.96	0.04			
0.350	3.81	0.06		Λ0 ($\frac{1}{2}$, $\frac{1}{2}$, ζ)	
0.425	3.71	0.06	0.100	3.75	0.15
0.500	3.78	0.05	0.400	4.60	0.10

[a]Evaluated from velocities of ultrasonic-wave propagation.

the dispersion curves. A force-constant model to serve for interpolation between the experimental points was developed. For CsCl structures the ΛA and ΛO branches are susceptibile to direct Fourier analysis in the manner suggested by Foreman and Lomer.[10] For these branches the following expression may be written:

$$2\pi^2 M_0 M_1 \nu^2_{A,O}(\vec{q}, \vec{j}) = \sum_{n=0}^{N} A_n \cos 2\pi n\zeta \ . \quad (1)$$

For other branches the following expression is appropriate:

$$2\pi^2 M_0 M_1 [\nu^2_A(\vec{q}, \vec{j}) + \nu^2_O(\vec{q}, \vec{j})] = \sum_{n=0}^{N} A_n \cos 2\pi n\zeta \ . \quad (2)$$

In these relationships, M_0 and M_1 are the atomic masses of the two different atomic species, ν is the frequency of the phonon with wave vector $\vec{q}$ and polarization $\vec{j}$, and the variable ζ is defined as q/q_{max}. The subscripts A and O refer to the acoustical and optical branches of the dispersion curves.

The Fourier coefficients $A_0, \ldots, A_n$ are themselves expressible as linear combinations of the interatomic force constants $\alpha^s_{i\sigma}$ and $\beta^s_{i\sigma}$. The α's and β's are, respectively, the diagonal and off-diagonal elements of the force-constant matrix, with s being the order of the stn nearest neighbor, i being an index associated with the directionality of atomic pair interactions, and σ being the interacting atomic species. The explicit relationships between the force constants and the Fourier coefficients are given in the Appendix. The notation follows that adopted by Squires[11] in his development of expressions for monatomic bcc and fcc lattices and has also been used by Gilat and Dolling[1] in analysis of their data for β-brass. The coefficients $A_1, \ldots, A_n$ can be described solely in terms of force interactions between like atoms, while the coefficients A_0 involve force interactions between both like and unlike atoms. Since the force interaction between two unlike atoms is unaffected by choice of coordinate origin at one atom or the other, it follows that $\alpha^s_{i0} = \alpha^s_{i1}$ and $\beta^s_{i0} = \beta^s_{i1}$ for unlike-neighbor interactions, so the σ subscript may be deleted. This deletion for unlike-neighbor interactions is practiced in Table II and in the Appendix.

Direct Fourier analyses of Eqs. (1) and (2) do not produce enough linearly independent relationships for good resolution of atomic force constants if interactions extend to fifth neighbor and beyond. Therefore, a nonlinear least-squares program[12] of the general form suggested by Boyter and McMurry[13] was developed to find a satisfactory set of atomic force constants. Best fits for the force constants were obtained by minimizing the variance ratio

$$V_R = \frac{1}{N_D - N_p} \sum_{i=1}^{N_D} \frac{(\nu_{i,c} - \nu_{i,0})^2}{(\delta\nu_{i,0})^2} \quad , \tag{3}$$

where N_D is the number of experimental phonon frequencies, N_p is the number of adjustable parameters, and $\nu_{i,c}$, $\nu_{i,0}$, and $\delta\nu_{i,0}$ are, respectively, the calculated value, observed value, and experimental uncertainty of the ith phonon frequency. It was found that a fifth-neighbor model with 20 constants produced reasonable fits for all branches of the dispersion curves except the ΛA and ΛO branches. The over-all fit, particularly to these last two branches, was significantly improved by expanding the force-constant model to 24 constants to include sixth-neighbor interactions. The fit was sufficiently good with inclusion of sixth-neighbor interactions to justify termination of effort, but the lack of perfection in the fit does indicate the presence of residual, still longer-range force interactions. The force constants for both the fifth-neighbor model and the sixth-neighbor model are shown in Table II, and dispersion curves are shown in Fig. 2, where the solid lines represent interpolation between the experimental points with the sixth-neighbor model.

TABLE II. Interatomic force constants for fifth- and sixth-neighbor force-constant models (units of dyn/cm).

	Fifth-neighbor model	Sixth-neighbor model		Fifth-neighbor model	Sixth-neighbor model
α_1^1	5788	6199	α_1^4	645	96
β_1^1	6723	6271	α_2^4	−36	5
α_{10}^2	5242	615	β_1^4	0	20
α_{11}^2	6244	8829	β_2^4	−244	143
α_{20}^2	−1042	−1261	α_{10}^5	546	1471
α_{21}^2	1719	2214	α_{11}^5	620	−168
α_{10}^3	−1366	−1249	β_{10}^5	1223	11
α_{11}^3	−271	−479	β_{11}^5	450	1236
α_{30}^3	2641	1243	α_{10}^6		5538
α_{31}^3	−1409	−202	α_{11}^6		−2631
β_{30}^3	430	−851	α_{20}^6		−723
β_{31}^3	−1134	−600	α_{21}^6		520

Variance ratio, fifth-neighbor model = 6.83
Variance ratio, sixth-neighbor model = 2.24

IV. DISCUSSION

A number of features that appear in the dispersion curves in Fig. 2 arise solely from symmetry and continuity constraints. A group-theoretical analysis of the CsCl lattice has been performed by Warren,[14] who has indicated which degeneracies must occur at the points of high symmetry. In metallic materials, screening of the macroscopic electric field by the conduction electrons results in an additional degeneracy between the LO and TO modes at the symmetry point Γ. Thus there is a degeneracy that is both required and observed in the dispersion curves for metallic CuZn and YZn but is not requisite in ionic materials and is not observed[15] in CsBr. At the symmetry point M, continuity requires that the $TO_1(\zeta, \zeta, 0)$ branch meet the $\Lambda O(\frac{1}{2}, \frac{1}{2}, \zeta)$ branch and the $TA_1(\zeta, \zeta, 0)$ branch meet the $\Lambda A(\frac{1}{2}, \frac{1}{2}, \zeta)$ branch, but the experimental degeneracy between these pairs of optical and acoustical branches, which was observed in β-

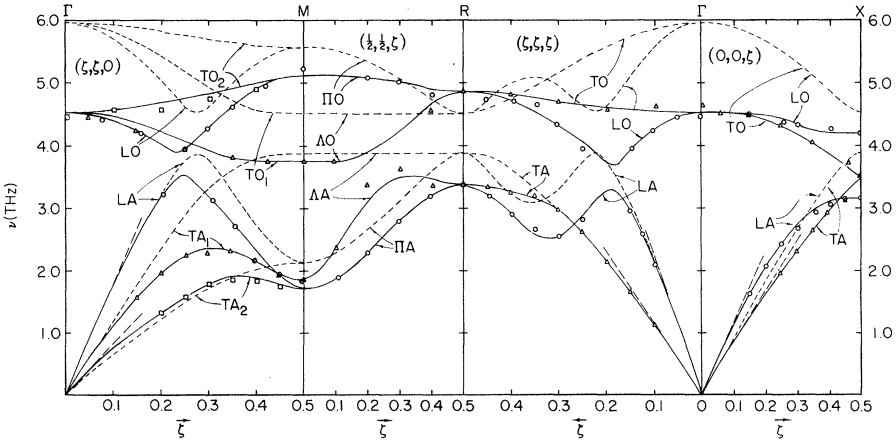

FIG. 2. Phonon distributions for YZn at room temperature along the principal symmetry directions. The solid lines represent dispersion curves fitted to the experimental points with a force-constant model including sixth-neighbor interactions. The dotted lines represent dispersion curves computed from a two-force-constant model involving only nearest-neighbor interactions with values for the force constants derived from single crystalline elastic constants. The dashed lines are limiting slopes at long-wavelength limits as indicated by measurements of ultrasonic wave velocities.

brass,[1] is not a symmetry requirement and does not occur for YZn. In fact, the observed splitting at M between these particular optical and acoustical branches in YZn is quite large and, while the mass difference between yttrium and zinc is a contributory factor, the degree of splitting in YZn can be shown to arise from interactions other than nearest neighbor. This is illustrated by the differences between the dotted and solid lines in Fig. 2. The dotted lines were generated with a nearest-neighbor model with two atomic force constants. Values for the two force constants of $\alpha_1^1 = 10999$ dyn/cm and $\beta_1^1 = 8071$ dyn/cm were obtained from a least-squares fit to the ultrasonic-wave velocities through the relations

$$(v_L^2/2a^2)(M_0+M_1) = \alpha_1^1 + \beta_1^1 , \tag{4a}$$

$$(v_1^2/2a^2)(M_0+M_1) = \alpha_1^1 , \tag{4b}$$

$$(v_2^2/2a^2)(M_0+M_1) = \alpha_1^1 - \beta_1^1 , \tag{4c}$$

where v_L, v_1, and v_2 are the longitudinal and shear wave velocities along the [110] direction, a is the lattice parameter, and the other quantities are as previously defined. Thus, differences between the dotted and solid lines in Fig. 2 reflect contributions from atomic force interactions of second through sixth neighbors, but in the sixth-neighbor model both fifth- and sixth-neighbor interactions vanish at the symmetry point M. Therefore, within this model the major portion of the splitting at M between the TO_2-ΛO optical branches and the TA_2-ΛA acoustical branches may be attributed to second- through fourth-neighbor interactions.

At the symmetry point X the experimental data for YZn indicate degeneracy of the TA(0, 0, ζ) and TO(0, 0, ζ) branches. A similar degeneracy was earlier observed in β-brass.[1] This is accidental degeneracy and is not required by symmetry, and such degeneracy does not occur in the limited phonon dispersion data which have been published[15] for CsBr. In β-brass the occurrence of this degeneracy, coupled with the near equality of the copper and zinc masses, yields the result noted by Gilat and Dolling[1] that copper-copper and zinc-zinc interactions must be very nearly equal. In YZn no such simple conclusion can be drawn owing to the large difference between the yttrium and zinc masses, though the degeneracy must be attributable to long-range forces arising from the valence electrons.

Reference to Fig. 2 shows that there is no evidence for a Kohn anomaly. However, the very pronounced splitting between the TO_1-ΛO and TA_1-ΛA branches at the point M created some suspicion of strong electron-phonon coupling so that a check for superconducting behavior was made. No superconductivity was detected down to 1.2 K.

It is widely recognized[16] that individual interatomic force constants $\alpha_{i\sigma}^s$ and $\beta_{i\sigma}^s$, which are generated from phonon dispersion data, are not physically meaningful as measures of atomic pair interactions but are simply fitting parameters. Comparison of values from fifth- and sixth-neighbor models in Table II shows appreciable variation between values for some of the constants. However, it should be emphasized that evaluation of the total resultant restoring force experienced by an atom displaced from equilibrium is much less sensitive to the number of neighbor interactions that are considered. Table III shows values for the restoring force resisting displacement along an axial direction from the nearest-neighbor model, the fifth-neighbor model, and the sixth-neighbor model. Values from fifth- and sixth-neighbor models agree to ~0.5% and are only 25–30% below values from the simplistic nearest-neighbor model. The implication is that the nearest-neighbor coordination shell dominates the force field but is modified by successive coordination shells with the degree of modification attenuating rapidly with increasing coordination shell number. Such dominance of the force field by near-neighbor coordination shells provides some justification and explanation for the fact that quasichemical approximations have been used with some success for estimating enthalpies of intermetallic phase formation.[17]

A phonon frequency distribution function $g(\nu)$ was calculated from the sixth-neighbor model by the method of Raubenheimer and Gilat.[18,19] This distribution function is shown in Fig. 3, and Van Hove singularities[20] are indicated by letters a–l. Debye temperature as a function of temperature was also calculated from the sixth-neighbor model. The result is shown in Fig. 4. Here it may be noted that θ_0 is 290.6 K, in reasonable accord with the value of 306.8 K from low-temperature elasticity data.[3] Elastic constants were computed from the interatomic force constants through the relations

$$C_{11} = (1/a)(2\alpha_1^1 + \alpha_{10}^2 + \alpha_{11}^2 + 4\alpha_{10}^3 + 4\alpha_{11}^3 + 18\alpha_1^4 + 4\alpha_2^4 + 4\alpha_{10}^5 + 4\alpha_{11}^5 + 4\alpha_{10}^6 + 4\alpha_{11}^6) ,$$

TABLE III. Net resultant restoring forces resisting atomic displacement along an axial direction (units of dyn/cm).

	Nearest-neighbor model	Fifth-neighbor model	Sixth-neighbor model
F_Y	87 991	61 208	61 558
F_{Zn}	87 991	67 408	67 788
$F_Y + F_{Zn}$	175 982	128 616	129 346

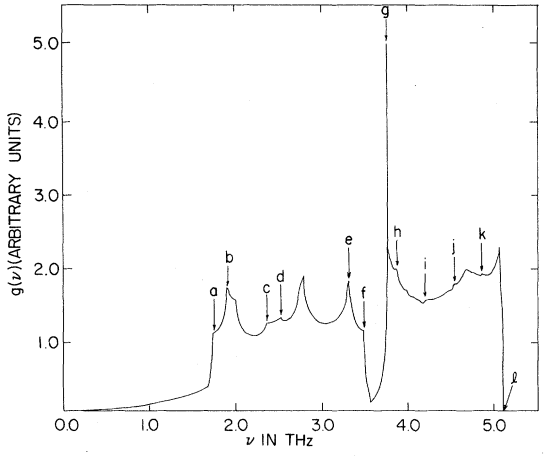

FIG. 3. Frequency distribution function calculated from the sixth-neighbor force-constant model. Van Hove singularities are indicated by a–l.

$$C_{12} = (1/a)\,(4\beta_1^1 + 4\beta_{30}^3 + 4\beta_{31}^3 + 4\beta_1^4 + 24\beta_2^4 + 8\beta_{10}^5 + 8\beta_{11}^5 - 2\alpha_1^1 - \alpha_{20}^2 - \alpha_{21}^2 - 2\alpha_{30}^3 - 2\alpha_{31}^3 - 2\alpha_{10}^3 - 2\alpha_{11}^3 - 2\alpha_1^4 - 20\alpha_2^4 - 4\alpha_{10}^5 - 4\alpha_{11}^5 - 4\alpha_{20}^6 - 4\alpha_{21}^6)\,,$$

$$C_{44} = (1/a)\,(2\alpha_1^1 + \alpha_{20}^2 + \alpha_{21}^2 + 2\alpha_{30}^3 + 2\alpha_{31}^3 + 2\alpha_{10}^3 + 2\alpha_{11}^3 + 2\alpha_1^4 + 20\alpha_2^4 + 4\alpha_{10}^5 + 4\alpha_{11}^5 + 4\alpha_{20}^6 + 4\alpha_{21}^6)\,.$$

Respective values of 9.38, 4.51, and 4.67 ($\times 10^{11}$ dyn/cm^2) compare favorably with values of 9.443, 4.600, and 4.731 ($\times 10^{11}$ dyn/cm^2) from ultrasonic data.[3] This comparison is quite acceptable when it is remembered that the three phonons that were generated from ultrasonic-wave propagation along the [110] direction were not given appreciably greater weight in evaluating the force constants than were the 108 INS phonons.

Finally, the mean-square vibrational amplitudes of both yttrium and zinc atoms were calculated from the sixth-neighbor model with summations being made for varying numbers of points in the irreducible zone. Because the frequency distribution function in Fig. 3 shows a strong minimum near 3.6 THz, which almost constitutes a gap in the distribution, it is meaningful to consider frequencies below this value as dominantly representative of acoustical modes and above this value as dominantly optical modes. It is therefore possible to divide the mean-square vibrational amplitudes into acoustical and optical contributions, and the results are shown in Table IV. Two features of this table seem significant. First, it seems quite reasonable to find $\langle u_Y^2\rangle_{\text{optical}}$ less than $\langle u_{Zn}^2\rangle_{\text{optical}}$, since this implies that the lighter zinc does most of the moving during out of phase vibration. Second, convergence is sufficiently slow to indicate that summation over a large number of points in the irreducible zone is necessary to obtain meaningful values for mean-square vibrational amplitudes.

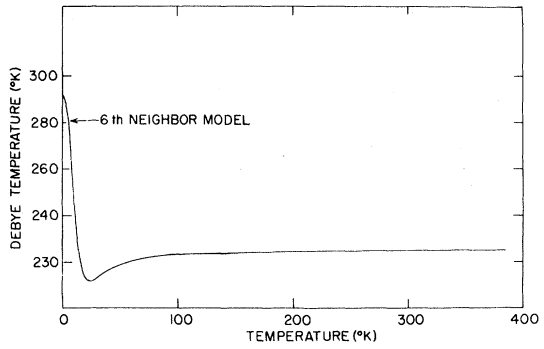

FIG. 4. Debye temperature as a function of temperature from the sixth-neighbor force-constant model.

APPENDIX

The Fourier coefficients A_n of Eqs. (1) and (2) are here expanded in terms of the atomic masses and the 24 independent atomic force constants, $\alpha_{i\sigma}^s$ and $\beta_{i\sigma}^s$, to include atomic interactions through sixth neighbor. The listing is by wave vector and mode.

1. $\vec{q} = (0, 0, \zeta)2\pi/a$; LA, LO modes:

$$A_0 = 4(\alpha_1^1 + \alpha_1^4 + 2\alpha_2^4)\,(M_0 + M_1) + M_0(\alpha_{11}^2 + 4\alpha_{11}^3 + 4\alpha_{11}^5 + \alpha_{11}^6) + M_1(\alpha_{10}^2 + 4\alpha_{10}^3 + 4\alpha_{10}^5 + \alpha_{10}^6)\,,$$

TABLE IV. Mean-square vibrational amplitudes of Y and Zn atoms along the [001] direction evaluated with the sixth-neighbor model (units of 10^{-18} cm^2).

No. of points in the irreducible zone	$\langle u_Y^2\rangle_{\text{acoustic}}$	$\langle u_Y^2\rangle_{\text{optical}}$	$\langle u_Y^2\rangle_{\text{total}}$	$\langle u_{Zn}^2\rangle_{\text{acoustic}}$	$\langle u_{Zn}^2\rangle_{\text{optical}}$	$\langle u_{Zn}^2\rangle_{\text{total}}$
35	0.603	0.062	0.665	0.403	0.241	0.644
84	0.696	0.070	0.767	0.467	0.276	0.743
220	0.781	0.078	0.859	0.524	0.307	0.832
680	0.857	0.085	0.942	0.577	0.335	0.913
1540	0.899	0.089	0.988	0.606	0.351	0.957
2925	0.925	0.092	1.017	0.624	0.361	0.985
4960	0.944	0.093	1.037	0.636	0.367	1.004

$$A_1 = -M_0(\alpha_{11}^2 + 4\alpha_{11}^3 + 4\alpha_{11}^5) - M_1(\alpha_{10}^2 + 4\alpha_{10}^3 + 4\alpha_{10}^5) ,$$

$$A_2 = -M_0\alpha_{11}^6 - M_1\alpha_{10}^6 .$$

2. $\vec{q} = (0, 0, \zeta)2\pi/a$; TA, TO, modes:

$$A_0 = 4(M_0 + M_1)(\alpha_1^1 + \alpha_1^4 + 2\alpha_2^4) + M_0(\alpha_{21}^2 + 2\alpha_{11}^3 + 2\alpha_{31}^3 + 4\alpha_{11}^5 + \alpha_{21}^6) + M_1(\alpha_{20}^2 + 2\alpha_{10}^3 + 2\alpha_{30}^3 + 4\alpha_{10}^5 + \alpha_{20}^6) ,$$

$$A_1 = -M_0(\alpha_{21}^2 + 2\alpha_{11}^3 + 2\alpha_{31}^3 + 4\alpha_{11}^5) - M_1(\alpha_{20}^2 + 2\alpha_{10}^3 + 2\alpha_{30}^3 + 4\alpha_{10}^5) ,$$

$$A_2 = -M_0\alpha_{21}^6 - M_1\alpha_{20}^6 .$$

3. $\vec{q} = (\zeta, \zeta, \zeta)2\pi/a$; LA, LO modes:

$$A_0 = 4(M_0 + M_1)(\alpha_1^1 + \alpha_1^4 + 2\alpha_2^4) + M_0(\alpha_{11}^2 + 2\alpha_{21}^2 + 2\alpha_{11}^3 + \alpha_{31}^3 + 2\beta_{31}^3 + 4\alpha_{11}^5 + \alpha_{11}^6 + 2\alpha_{21}^6) + M_1(\alpha_{10}^2 + 2\alpha_{20}^2 + 2\alpha_{10}^3 + \alpha_{30}^3 + 2\beta_{31}^3 + 4\alpha_{10}^5 + \alpha_{10}^6 + 2\alpha_{20}^6) ,$$

$$A_1 = -M_0(\alpha_{11}^2 + 2\alpha_{21}^2 + 3\alpha_{11}^5 - 2\beta_{11}^5) - M_1(\alpha_{10}^2 + 2\alpha_{20}^2 + 3\alpha_{10}^5 - 2\beta_{10}^5) ,$$

$$A_2 = -M_0(2\alpha_{11}^3 + \alpha_{31}^3 + 2\beta_{31}^3 + \alpha_{11}^6 + 2\alpha_{21}^6) - M_1(2\alpha_{10}^3 + \alpha_{30}^3 + 2\beta_{30}^3 + \alpha_{10}^6 + 2\alpha_{20}^6) ,$$

$$A_3 = -M_0(\alpha_{11}^5 + 2\beta_{11}^5) - M_1(\alpha_{10}^5 + 2\beta_{10}^5) .$$

4. $\vec{q} = (\zeta, \zeta, \zeta)2\pi/a$; TA, TO modes:

$$A_0 = 4(M_0 + M_1)(\alpha_1^1 + \alpha_1^4 + 2\alpha_2^4) + M_0(\alpha_{11}^2 + 2\alpha_{21}^2 + 2\alpha_{11}^3 + \alpha_{31}^3 + 4\alpha_{11}^5 - \beta_{31}^3 + \alpha_{11}^6 + 2\alpha_{21}^6) + M_1(\alpha_{10}^2 + 2\alpha_{20}^2 + 2\alpha_{10}^3 + \alpha_{30}^3 - \beta_{30}^3 + 4\alpha_{10}^5 + \alpha_{10}^6 + 2\alpha_{20}^6) ,$$

$$A_1 = -M_0(\alpha_{11}^2 + 2\alpha_{21}^2 + 3\alpha_{11}^5 + \beta_{11}^5) - M_1(\alpha_{10}^2 + 2\alpha_{20}^2 + 3\alpha_{10}^5 + \beta_{10}^5) ,$$

$$A_2 = -M_0(2\alpha_{11}^3 + \alpha_{31}^3 - \beta_{31}^3 + \alpha_{11}^6 + 2\alpha_{21}^6) - M_1(2\alpha_{10}^3 + \alpha_{30}^3 - \beta_{30}^3 + \alpha_{10}^6 + 2\alpha_{20}^6) ,$$

$$A_3 = -M_0(\alpha_{11}^5 - \beta_{11}^5) - M_1(\alpha_{10}^5 - \beta_{10}^5) .$$

5. $\vec{q} = (\zeta, \zeta, 0)2\pi/a$; LA, LO modes:

$$A_0 = 4(M_0 + M_1)(\alpha_1^1 + \alpha_1^4 + 2\alpha_2^4) + M_0(\alpha_{11}^2 + \alpha_{21}^2 + 3\alpha_{11}^3 + 2\alpha_{31}^3 + \beta_{31}^3 + 2\alpha_{11}^5 + 2\beta_{11}^5 + \alpha_{11}^6 + \alpha_{21}^6) + M_1(\alpha_{10}^2 + \alpha_{20}^2 + 3\alpha_{10}^3 + 2\alpha_{30}^3 + \beta_{30}^3 + 2\alpha_{10}^5 + 2\beta_{10}^5 + \alpha_{10}^6 + \alpha_{20}^6) ,$$

$$A_1 = -M_0(\alpha_{11}^2 + \alpha_{21}^2 + 2\alpha_{11}^3 + 2\alpha_{31}^3) - M_1(\alpha_{10}^2 + \alpha_{20}^2 + 2\alpha_{10}^3 + 2\alpha_{30}^3) ,$$

$$A_2 = -M_0(\alpha_{11}^3 + \beta_{31}^3 + 2\alpha_{11}^5 + 2\beta_{11}^5 + \alpha_{11}^6 + \alpha_{21}^6) - M_1(\alpha_{10}^3 + \beta_{30}^3 + 2\alpha_{10}^5 + 2\beta_{10}^5 + \alpha_{10}^6 + \alpha_{20}^6) .$$

6. $\vec{q} = (\zeta, \zeta, 0)2\pi/a$; TA_1, TO_1 modes:

$$A_0 = 4(M_0 + M_1)(\alpha_1^1 + \alpha_1^4 + 2\alpha_2^4) + M_0(2\alpha_{21}^2 + 4\alpha_{11}^3 + \alpha_{31}^3 + 2\alpha_{11}^5 + 2\alpha_{21}^6) + M_1(2\alpha_{20}^2 + 4\alpha_{10}^3 + \alpha_{30}^3 + 2\alpha_{10}^5 + 2\alpha_{20}^6) ,$$

$$A_1 = -M_0(2\alpha_{21}^2 + 4\alpha_{11}^3) - M_1(2\alpha_{20}^2 + 4\alpha_{10}^3) ,$$

$$A_2 = -M_0(\alpha_{31}^3 + 2\alpha_{11}^5 + 2\alpha_{21}^6) - M_1(\alpha_{30}^3 + 2\alpha_{10}^5 + 2\alpha_{20}^6) .$$

7. $\vec{q} = (\zeta, \zeta, 0)2\pi/a$; TA_2, TO_2 modes:

$$A_0 = 4(M_0 + M_1)(\alpha_1^1 + \alpha_1^4 + 2\alpha_2^4) + M_0(\alpha_{11}^2 + \alpha_{21}^2 + 3\alpha_{11}^3 + 2\alpha_{31}^3 - \beta_{31}^3 + 2\alpha_{11}^5 - 2\beta_{11}^5 + \alpha_{11}^6 + \alpha_{21}^6) + M_1(\alpha_{10}^2 + \alpha_{20}^2 + 3\alpha_{10}^3 + 2\alpha_{30}^3 - \beta_{30}^3 + 2\alpha_{10}^5 + \alpha_{10}^6 + \alpha_{20}^6 - 2\beta_{10}^5) ,$$

$$A_1 = -M_0(\alpha_{11}^2 + \alpha_{21}^2 + 2\alpha_{11}^3 + 2\alpha_{31}^3) - M_1(\alpha_{10}^2 + \alpha_{20}^2 + 2\alpha_{10}^3 + 2\alpha_{30}^3) ,$$

$$A_2 = -M_0(\alpha_{11}^3 - \beta_{31}^3 + 2\alpha_{11}^5 - 2\beta_{11}^5 + \alpha_{11}^6 + \alpha_{21}^6) - M_1(\alpha_{10}^3 - \beta_{30}^3 + 2\alpha_{10}^5 - 2\beta_{10}^5 + \alpha_{10}^6 + \alpha_{20}^6) .$$

8. $\vec{q} = (\frac{1}{2}, \frac{1}{2}, \zeta)2\pi/a$; ΠA, ΠO modes:

$$A_0 = 4(M_0 + M_1)(\alpha_1^1 + \alpha_1^4 + 2\alpha_2^4) + M_0(2\alpha_{11}^2 + 3\alpha_{21}^2 + 2\alpha_{11}^3 + 2\alpha_{31}^3 + 4\alpha_{11}^5 + \alpha_{21}^6) + M_1(2\alpha_{10}^2 + 3\alpha_{20}^2 + 2\alpha_{10}^3 + 2\alpha_{30}^3 + 4\alpha_{10}^5 + \alpha_{20}^6) ,$$

$$A_1 = -M_0(\alpha_{21}^2 - 2\alpha_{11}^3 - 2\alpha_{31}^3 + 4\alpha_{11}^5) - M_1(\alpha_{20}^2 - 2\alpha_{10}^3 - 2\alpha_{30}^3 + 4\alpha_{10}^5) ,$$

$$A_2 = -M_0\alpha_{21}^6 - M_1\alpha_{20}^6 .$$

9. $\vec{q} = (\frac{1}{2}, \frac{1}{2}, \zeta)2\pi/a$; ΛO mode:

$$A_0 = M_0(4\alpha_1^1 + 4\alpha_1^4 + 8\alpha_2^4 + 4\alpha_{21}^2 + \alpha_{11}^2 + 4\alpha_{11}^3 + 4\alpha_{11}^5 + \alpha_{11}^6) ,$$

$$A_1 = -M_0(\alpha_{11}^2 - 4\alpha_{11}^3 + 4\alpha_{11}^5) ,$$

$$A_2 = -M_0\alpha_{11}^6 .$$

10. $\vec{q} = (\frac{1}{2}, \frac{1}{2}, \zeta)2\pi/a$; ΛA mode:

$$A_0 = M_1(4\alpha_1^1 + 4\alpha_1^4 + 8\alpha_2^4 + 4\alpha_{20}^2 + \alpha_{10}^2 + 4\alpha_{10}^3 + 4\alpha_{10}^5 + \alpha_{10}^6) ,$$

$$A_1 = -M_1(\alpha_{10}^2 - 4\alpha_{10}^3 + 4\alpha_{10}^5) ,$$

$$A_2 = -M_1\alpha_{10}^6 .$$

---

*Present address: Sandia Corporation, Albuquerque, N. M. 87115.

[1]G. Gilat and G. Dolling, Phys. Rev. 138, A1053 (1965).

[2]M. Hansen and K. Anderko, *Constitution of Binary Alloys* (McGraw-Hill, New York, 1958), pp. 241–243.

[3]R. J. Schiltz, Jr., T. S. Prevender, and J. F. Smith, J. Appl. Phys. 42, 4680 (1971).

[4]W. B. Pearson, *A Handbook of Lattice Spacings and Structures of Metals and Alloys* (Pergamon, New York, 1967), Vol. 2, p. 1287.

[5]M. D. Goldberg, S. F. Mughabghab, S. N. Purohit, B. J. Magurno, and V. M. May, U. S. Atomic Energy Commission Report No. BNL-325, 2nd ed., Suppl. No.

2, Vol. II A, 1966 (unpublished).
[6]P. Chiotti, J. T. Mason, and K. J. Gill, Trans. AIME 221, 573 (1961).
[7]J. P. Jan, Division of Pure Physics, National Research Council, Ottawa, Canada (private communication).
[8]B. N. Brockhouse, in *Inelastic Scattering of Neutrons in Solids and Liquids* (International Atomic Energy Agency, Vienna, 1961), p. 113.
[9]T. O. Brun and S. K. Sinha (unpublished).
[10]A. J. E. Foreman and W. M. Lomer, Proc. Phys. Soc. (London) 70, 1143 (1957).
[11]G. L. Squires, in *Inelastic Scattering of Neutrons in Solids and Liquids* (International Atomic Energy Agency, Vienna, 1963), Vol. II, p. 125.
[12]T. S. Prevender, U. S. Atomic Energy Commission Report No. IS-2185, 1969 (unpublished).
[13]J. K. Boyter and H. L. McMurry, U. S. Atomic Energy Commission Report No. IN-1148, 1967 (unpublished).
[14]J. L. Warren, Rev. Mod. Phys. 40, 38 (1968).
[15]J. Daubert, Phys. Letters 32A, 437 (1970).
[16]R. S. Leigh, B. Szigeti, and V. K. Tewary, Proc. Roy. Soc. (London) A320, 505 (1971).
[17]See, e.g., O. Kubaschewski, in *The Physical Chemistry of Metallic Solutions and Intermetallic Compounds* (Her Majesty's Stationery Office, London, 1959), Paper 3C.
[18]L. J. Raubenheimer and G. Gilat, U. S. Atomic Energy Commission Report No. ORNL-TM-1425, 1966 (unpublished).
[19]G. Gilat and L. J. Raubenheimer, Phys. Rev. 144, 390 (1966).
[20]L. Van Hove, Phys. Rev. 89, 1189 (1953).

PHYSICAL REVIEW B VOLUME 6, NUMBER 12 15 DECEMBER 1972

Localized *d* States for Pseudopotential Calculations: Application to the Alkaline-Earth Metals*

John A. Moriarty
University of California, Los Alamos Scientific Laboratory, Los Alamos, New Mexico 87544
(Received 24 July 1972)

A procedure for constructing very localized *d* basis states for generalized pseudopotential calculations is suggested and applied to the alkaline-earth metals calcium, strontium, and barium. Unlike the *d* states of the free ion or atom, these localized *d* states do not significantly overlap their neighbors in the metal. They also appear to lead to more accurate estimates of the *s*-*d* hybridization. Form factors and energy–wave-number characteristics are calculated and used to study the effects of hybridization on representative physical properties of the alkaline earths. In general, hybridization is found to make important contributions to the liquid-metal resistivity and the low-temperature-phase stability, but not to the binding energy nor to the phonon frequencies. A preliminary calculation also suggests that the fcc-bcc phase transitions in calcium and strontium can be understood in terms of the generalized pseudopotential theory.

I. INTRODUCTION

The generalization of pseudopotential theory to the *d*-band metals[1-3] relies on a power-series expansion of the electron density and the total energy in each of two small quantities. The first of these quantities is a pseudopotential w_0, which is exactly analogous to the pseudopotential entering the simple-metal theory. The second is a hydridization potential Δ, which embodies the fact that ionic or atomic *d* states are not good eigenstates of the crystal Hamiltonian H. Formally, if one defines a set of localized *d* states $|\varphi_d\rangle$ by the Schrödinger equation

$$H^i|\varphi_d\rangle = E_d^i|\varphi_d\rangle , \tag{1}$$

then the hybridization potential Δ can be expressed in the form

$$\Delta = \delta V - \langle\varphi_d|\delta V|\varphi_d\rangle , \tag{2}$$

where

$$\delta V = H^i - H . \tag{3}$$

In principle, one is free to choose H^i at will, so long as the $|\varphi_d\rangle$ remain orthogonal to the core states of the metal $|\varphi_c\rangle$ (which are assumed to be eigenfunctions of H). In a given calculation, if one were to keep terms of all orders in w_0 and Δ, then the result would be independent of the choice of H^i. Of course, one always wishes to terminate these expansions at a finite order (e.g., first order in Δ^2 and w_0 for the electron density and second order in these quantities for the total energy), and thus the result one obtains will generally reflect the choice of H^i.

In practice, the most obvious procedure is to take H^i as the Hamiltonian of the free ion or atom, as we did recently with the noble metals.[4,5] Then δV is, for example, the difference in potential seen by an electron in a free ion and an electron in the vicinity of an ion site in the metal, and the hybridization potential Δ can be expected to be small, at least inside the core region of the ion. Free-ion *d* states, however, may extend well out-